

Evaluation of Passive Millimeter Wave System Performance in Adverse Weather Conditions

N. Gopalsami, S. Liao*, T. Elmer, E. R. Koehl, and A. C. Raptis
Argonne National Laboratory, Lemont, IL, USA 60439

ABSTRACT

Passive millimeter wave (PMMW) imaging has shown distinct advantages for detection of terrestrial targets under optically obscuring conditions such as cloud, haze, snow, and light rain. The purpose of this paper is to evaluate the performance of a PMMW imager for terrestrial target recognition with respect to range of detection and climatic variables such as cloud, light rain, and snow. We used a dual polarization MMW radiometer in the frequency range of 70-100 GHz for the evaluation. We present experimental results and analyze the effect of weather conditions on the image quality and its polarization contrast. These results will be useful for quantitative prediction of PMMW system performance for long-range terrestrial imaging.

Keywords: passive, millimeter wave, radiometer, imaging, polarization, weather

1. INTRODUCTION

Passive millimeter-wave (PMMW) imaging is an active area of research for applications in terrestrial remote sensing, radioastronomy, and airport security.¹⁻⁴ PMMW imaging has a better temperature contrast in outdoor environments than indoors owing to the cold sky background. The ground targets appear colder from the sky-reflected radiation. For example, the apparent temperature of the sky background at 94 GHz is 70 K in comparison to 220 K at infrared wavelengths in clear weather. In addition, the polarization diversity of PMMW radiation may be used for enhanced discrimination of targets.

While optical systems (visible and IR) require clear atmospheric conditions for reliable operation, PMMW imaging is relatively immune to weather conditions such as cloud, fog, snow, and light rain. For example, the atmospheric attenuation in the range of millimeter wave (MMW) frequencies is 0.07 to 3 dB/km in drizzle and fog conditions, whereas it is one to three orders of magnitude higher at optical frequencies (exceeding 100 dB/km in foggy conditions).^{5,6}

In this paper, we evaluated the imaging performance of a dual polarization, 70-100 GHz radiometer on various weather conditions including clear, rainy, and snowy days. Experiments were conducted on different outdoor scenes including a car at 10 m and a dome shaped building at 300 m from the imager. The results were analyzed to determine the image resolution, image quality, and polarization contrast. This paper is organized as follows: The outdoor experimental setup is presented in Section 2, followed by the experimental results and analysis in Section 3, and conclusions in Section 4.

2. OUTDOOR PMMW EXPERIMENTAL SETUP

A schematic diagram of PMMW experimental setup for outdoor imaging is shown in Fig. 1. A 2-axis translational stage is used to raster scan a 6-inch (15.24-cm) imaging lens to focus the scene onto a 70-100 GHz dual polarization radiometer (Fig. 2). A wire grid polarizer splits the incoming signal into vertically and horizontally polarized signal paths. The signal in each path is received by a circular corrugated antenna and undergoes identical signal processing chains comprised of a 70 – 100 GHz band pass filter, a low noise amplifier, a Schottky barrier diode detector, and a baseband video amplifier. The baseband signals are collected by a DAQ system using a LabVIEW program running on a laptop. The radiometer can operate either in total power or Dicke-switched modes; the latter uses a chopper in front of the beam splitter.

*sliao@anl.gov ; phone: 630-252-9204; fax: 630-252-3250

2.1 Radiometric Model

The apparent temperature T_R measured by the radiometer for a terrestrial scene in Fig. 3 can be approximated as:

$$T_R = (1 - \varepsilon)[(1 - e^{-\tau_a})T_{atm} + e^{-\tau_a}T_{sky}] + \varepsilon e^{-\tau_t}T_t, \quad (1)$$

where T_{sky} , T_{atm} , and T_t are real temperatures of the sky, atmosphere, and target, respectively, τ_a and τ_t are the integrated attenuation of the atmosphere between the sky and the target and between the target and the radiometer, respectively, and ε is the emissivity of the target. The image contrast is affected by the atmospheric effects depending on the level of attenuation coefficient τ_a . Because of relatively short distances of the target from the radiometer, τ_t may be neglected. Considering the case, when $\tau_a=0$ (clear sky) and $\varepsilon=0$ (e.g., metal), the contrast is the highest as T_R equals T_{sky} . On the other hand, the contrast is the lowest when $\tau_a \sim \infty$ and $\varepsilon=1$ (e.g., asphalt), T_R equals T_t . The attenuation coefficients at 94 GHz for drizzle (0.25 mm/h), fog (0.1 g/m³), and heavy rain (25 mm/h) are on the order of 0.2 dB/km, 0.5 dB/km, and 10 dB/km.⁵ Assuming $T_{sky} = 70\text{K}$ and $T_{atm}=290\text{K}$, the apparent temperatures of a metallic target for these weather conditions are estimated as: 115K, 166K, and 290K, respectively. Thus the image contrast is reduced to nearly zero during heavy rain, but not severely affected by fog and light drizzle.

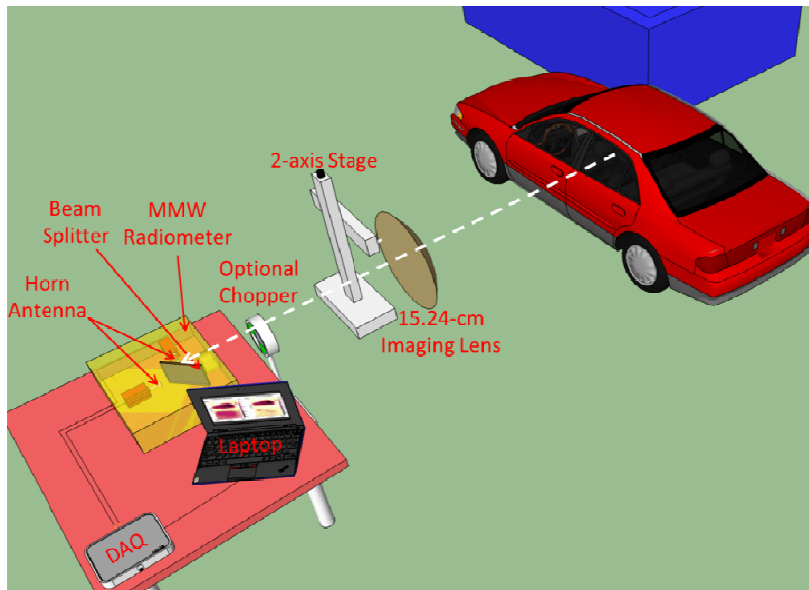


Figure 1. PMMW experimental setup outdoor imaging (Objects not to scale).

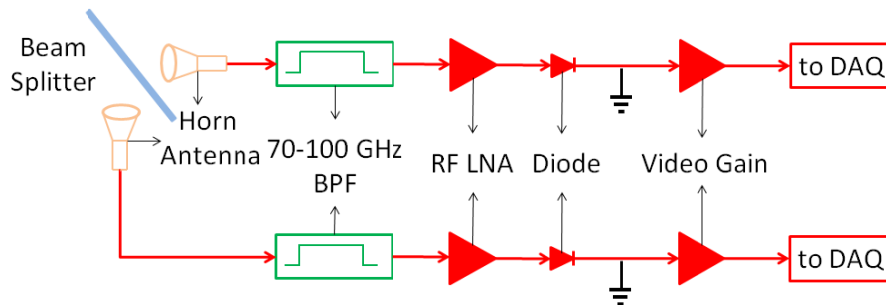


Figure 2. Architecture of dual-polarization 70-100 GHz radiometer.

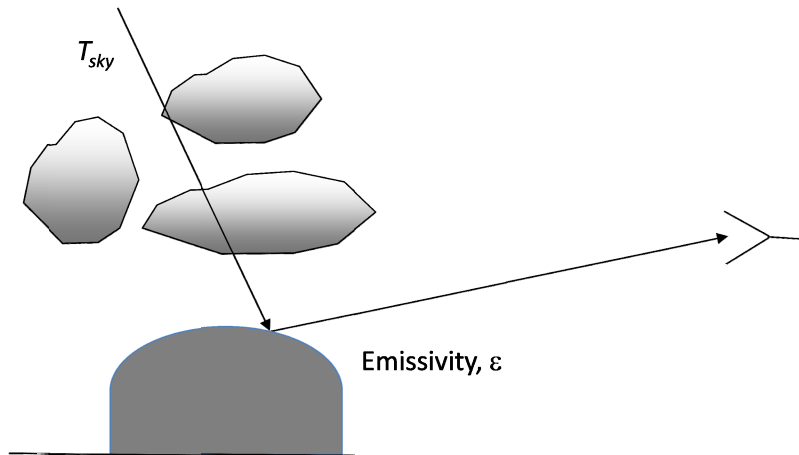


Figure 3. Radiometric model of a scene for a down looking radiometer.

3. EXPERIMENTAL RESULTS AND ANALYSIS

We performed a series of outdoor images of different scenes at different distances under various weather conditions, including 1) clear day, 2) cloudy day, 3) rainy day, and 4) snowy day. The imaging scenes included a car at 5 m and 10 m, and a dome-shaped building at 300 m from the radiometer.

3.1 Clear day

During clear days, we acquired images of a car at 10 m and a domed building at 300 m to evaluate the effect of target distance on image quality. Figure 4 gives passive MMW images (sum of both horizontal and vertical polarizations) of the car (Fig. 4a) and the dome (Fig. 4b) overlaid on optical images of the scenes. An augmented reality technique was used to match the two disparate images based on known markers in the scene. The integration time for the 10-m away 2001 red Nissan Altima car was 1 s and for the 300-m-away dome was 0.5 s.⁷ The sky background temperature (Fig. 4b) is much colder (darker in color) than objects at ambient temperature (building, ground, and electrical poles). Also, objects with higher reflectivity such as metallic objects reflect cold sky background well and thus appear colder (car body, dumpster, ventilation fans, and dome). For a given antenna, the resolution (antenna footprint) varies with the distance and its beam angle. Consequently, small features such as the window frame and wheels of the car are recognizable at 10 m distance as well as the light poles at ~20 m in Fig. 3b, but the large (~30 m diameter) dome at 300m distance is only tens of pixels across. Table 1 gives the performance comparison of scenes for the three ranges with our system using 15.24cm diameter lens. The long imaging time may be effectively reduced by a factor 10 or more without losing information using compressive sensing.^{8,9}

Table 1. Performance of PMMW imager at 3 ranges with 15.24-cm lens

Object distance	5 m	10 m	300 m
Object imaged	Car	Car	Dome
Integration time	0.5 s	0.5 s	0.5 s
Noise-equivalent delta temperature	0.17K	0.17K	0.17K
Object resolution	8 cm	16 cm	4.8 m
Field of view	8 x 8 m	16 x 16 m	480 x 480 m
Image pixels	100 x 100	100 x 100	100 x 100
Imaging Time (raster scan)	3 h	3 h	3 h

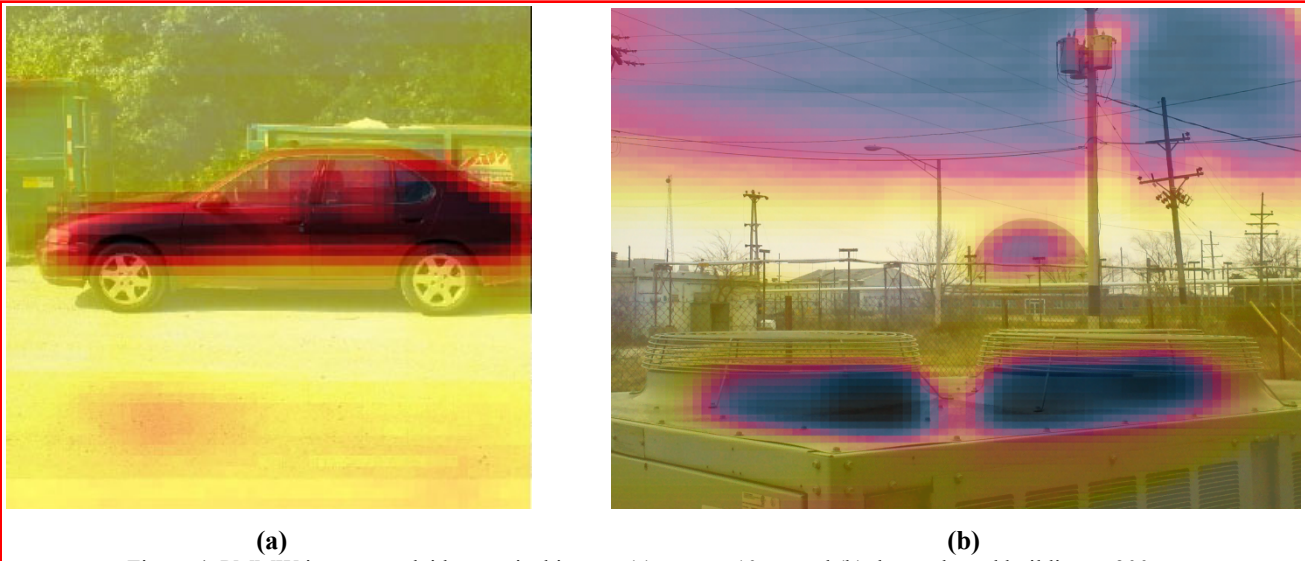


Figure 4. PMMW image overlaid on optical image: (a) a car at 10 m; and (b) dome-shaped building at 300 m.

3.2 Cloudy day

Figure 5 compares the images on a clear day and a cloudy day for the 300-m distant dome scene (the visual image is shown in Fig. 4b for reference). The images on a clear day (Figs. 5a and 5b) contain more polarization contrast than that those on a cloudy day (Figs. 5c and 5d). Notably, the ground temperature for the horizontal image on a clear day in Fig. 5a is much colder than that for the vertical polarization image in Fig. 5b, while the ground temperature for both polarizations on a cloudy day is not that much different. This is due to the relatively small temperature contrast between clouds and the ground on a cloudy day, which reduces the contribution to the image contrast due to reflection. Note also that the background sky appears colder at higher elevation than near horizon because of path length difference.

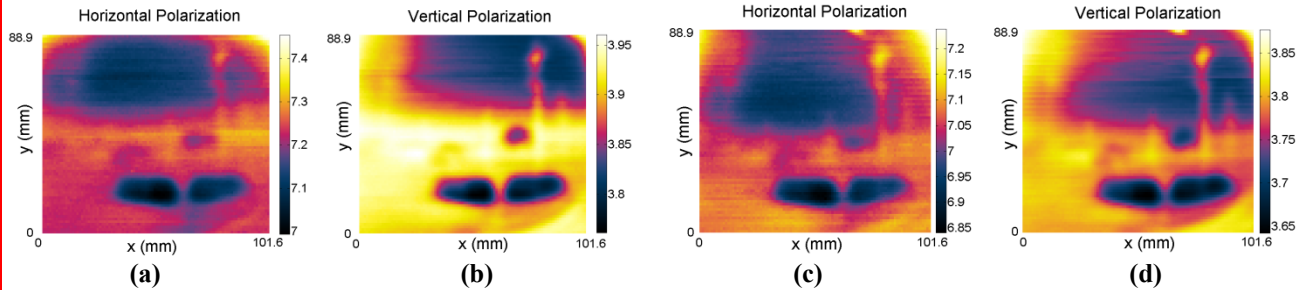


Figure 5. Comparison of horizontal and vertical polarized images of 300-m distant dome scene on a clear day ((a) and (b)) and a cloudy day ((c) and (d)).

3.3 Rainy day

Figure 6 gives dual-polarization images of a car during light rain and after the rain stopped, respectively (the visual image is shown in Fig. 4a). During rain, the apparent temperature of the scene is higher, as shown in Figs. 6a and 6b. This is because the rain droplets emit millimeter waves at outdoor ambient temperature as well as attenuates the cold sky radiation. Also, the reflection of the car by the ground is clearly seen in the horizontal polarization, (Fig. 6c), but not so clear in the vertical polarization (Fig. 6d), which can be explained by the reflection formulas below:^{7,10}

$$R^H = \left| \frac{\eta_2 \cos \theta_i - \eta_1 \cos \theta_t}{\eta_2 \cos \theta_i + \eta_1 \cos \theta_t} \right|^2 \quad (2a)$$

$$R^V = \left| \frac{\eta_2 \cos \theta_t - \eta_1 \cos \theta_i}{\eta_2 \cos \theta_t + \eta_1 \cos \theta_i} \right|^2, \quad (2b)$$

where $\sin(\theta_t) = \gamma_{Air} / \gamma_{Ground} \sin(\theta_i)$; $\gamma \equiv j\omega\sqrt{\mu_0\epsilon_0(\epsilon' - j\epsilon'')}$; R^H and R^V are the reflection coefficients for the horizontal and vertical polarization signals, respectively; η_1 and η_2 are wave impedances of air and ground, respectively; and θ_i is the incident angle of the rays at the interface. From Eq. (2b), Brewster phenomenon exists for vertical polarization. Near the Brewster angle, the reflection of the vertical polarization is much lower than that of the horizontal polarization. For a dry ground permittivity of $\epsilon_{Ground} = 3.5$, the Brewster angle for the vertical polarization is $\theta_B = \arctan[\sqrt{\epsilon_{Ground}}] \sim 62^\circ$.

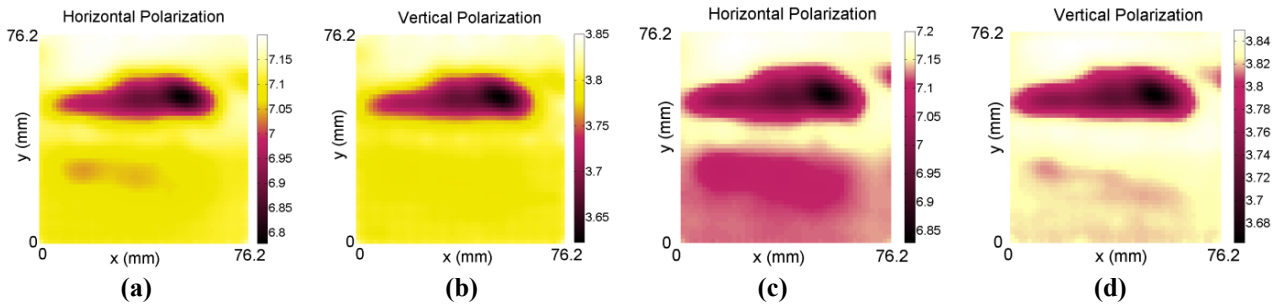


Figure 6. Dual-polarization PMMW images during light rain ((a) and (b)) and after rain stopped ((c) and (d)).

3.4 Snowy day

Figure 7 shows the visual and PMMW images of a Buick Regal LS 1999 car 5 m away in front of a metallic fence during and after the snow stopped but accumulated on surfaces. As can be seen from Fig. 7c, the horizontal MMW image is blurred due to snowflakes. Also, the sky background temperature appears hotter during snow in Figs. 7a and 7b compared to that after snow stopped in Figs. 7e and 7f, which is due to the MMW emission of the snowflakes. Similarly, the ground temperature appears hotter due to accumulation of snow on the ground. Finally a thin layer of snow accumulation on the car body doesn't affect the MMW image significantly. These results show that PMMW imaging may be effectively used for terrestrial imaging during or after snow accumulation on surfaces.

4. CONCLUSIONS

We have evaluated the performance of passive millimeter wave system for terrestrial imaging of targets with respect to target distance and under various weather conditions including clear, cloudy, rainy and snowy days. Three different ranges have been tested, 5m, 10m, and 300m. The imaging results for all the cases tested show varying degrees of image quality but yet acceptable images for target recognition. The cloud, snow, and rain attenuate the millimeter waves increasingly due to droplet scattering and in turn decrease the image contrast in both polarizations. The sky background reflection is found to be the most important contribution to the PMMW image contrast. Solid objects with high reflectivity appear colder due to the reflection of the cold sky background temperature. The ground terrain appears to be a good reflector for MMWs, as was evident from the PMMW images of a car at short distances away.

Acknowledgements

This work is supported by the office of Nonproliferation and Verification Research and Development under the National Nuclear Security Administration of the U.S. Department of Energy under Contract No. DE-AC02-06CH11357.

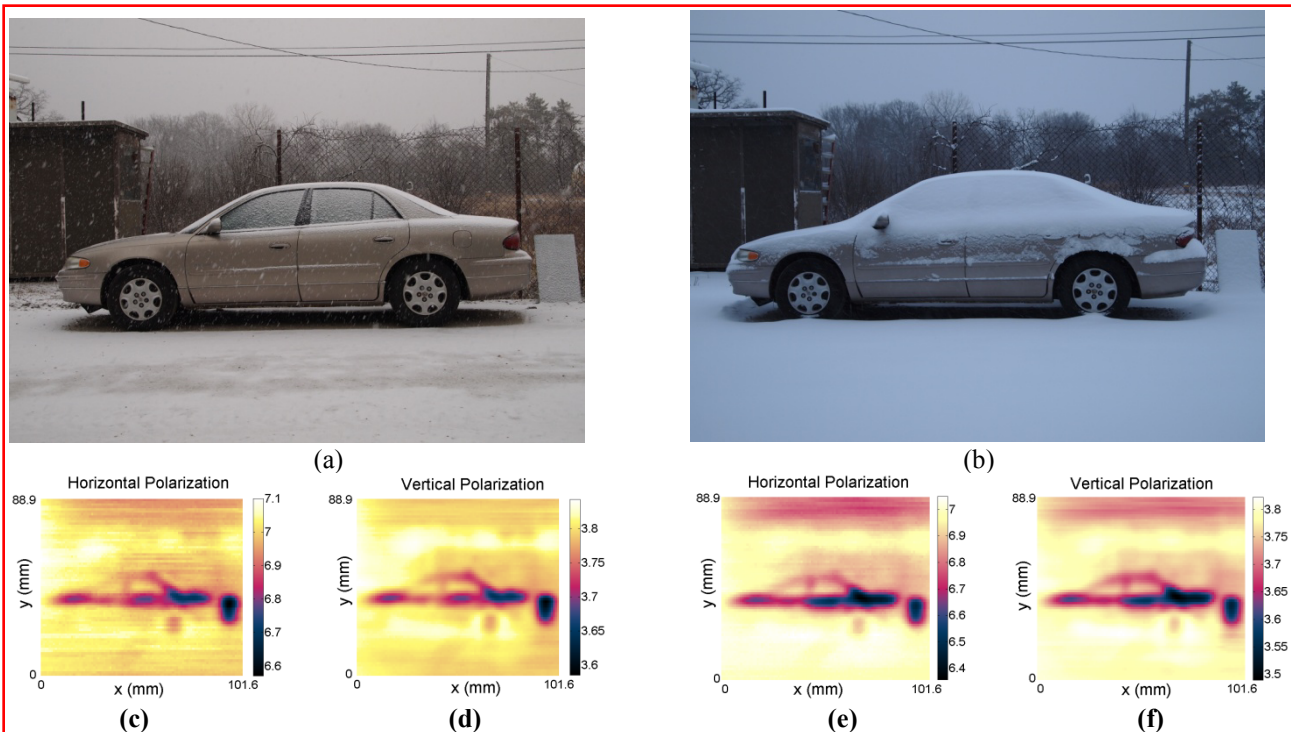


Figure 7. Visual images ((a), during snow and (b), after snow stopped) and PMMW images of a car at 5-m distance during ((c), horizontal pol and (d), vertical pol) and after snow stopped ((e), horizontal pol and (f), vertical pol).

REFERENCES

- [1] Janssen, M. A., Ed., [Atmospheric Remote Sensing by Microwave Radiometry], New York: Wiley (1993).
- [2] Lynch, J. J., Macdonald, P. A., Moyer, H. P., and Nagele, R. G., "Passive millimeter wave imaging sensors for commercial markets," *Applied Optics*, Vol. 49, No. 19 (2010).
- [3] Fetterman, M. R., Grata, J., Jubic, J. G., Kiser, Jr., W. L., and Visnansky, A., "Simulation, acquisition, and analysis of passive millimeter-wave images in remote sensing applications," *Optics Express*, 16, 20503-20515 (2008).
- [4] Peichl, M., Dill, S., Jirousek, M., Anthony, J. W., and Sub, H., "Fully-polarimetric passive mmW imaging systems for security applications," *Proc. SPIE 7837*, 78370C (2010).
- [5] Yujiri, L., Shoucri, M., and Moffa, P., "Passive millimeter-wave imaging," *IEEE Microwave Magazine*, September, (2003).
- [6] Appleby, R., and Anderton, R. N., "Millimeter-wave and submillimeter-wave imaging for security and surveillance," *Proc. IEEE*, 95, 1683-1690 (2007).
- [7] Liao, S., Gopalsami, N., Elmer, T. W., Koehl, E. R., Heifetz, A., Avers, K., Dieckman, E., and Raptis, A. C., "Passive millimeter-wave dual-polarization imagers," *IEEE Transactions on Instrumentation and Measurement*, vol. 99 (2012).
- [8] Gopalsami, N., Elmer, T. W., Liao, S., Ahern, R., Heifetz, A., and Raptis, A. C., "Compressive Sampling in Passive Millimeter Wave Imaging," *Proc. of SPIE*, vol. 8022, pp. 80220I-1: 80220I-1-6 (2011).
- [9] Babacan, S. D., Luessi, M., Spinoulas, L., Katassgelos, A. K., Gopalsami, N., Elmer, T. W., Ahern, R., Liao, S., and Raptis, A. C., "Compressive Passive Millimeter Wave Imaging," *IEEE International Conference in Image Processing (ICIP)*, Brussels, Belgium, September (2011).
- [10] Balanis, C. A., [Advanced Engineering Electromagnetics], John Wiley & Sons, Inc. (1998).